ELSEVIER

Contents lists available at ScienceDirect

Environmental and Sustainability Indicators

journal homepage: www.sciencedirect.com/journal/environmental-and-sustainability-indicators



Exploring characteristics and drivers of flood hazard under different urban development patterns

Ming Zhong a,b,* o, Tailin Chen a, Lu Zhuo c, Zeqiang Wang b, Feng Ling d, Dawei Han b

- a School of Geography and Planning, Sun Yat-Sen University & Southern Marine Science and Engineering Guangdong Laboratory (Zhuhai), Zhuhai, 519000, China
- ^b School of Civil, Aerospace, and Design Engineering, University of Bristol, Bristol, UK
- ^c School of Earth and Environmental Sciences, Cardiff University, Cardiff, UK
- d Chinese Academy of Sciences Key Laboratory of Monitoring and Estimate for Environment and Disaster of Hubei Province, Innovation Academy for Precision Measurement Science and Technology, Chinese Academy of Sciences, Wuhan, 430071, China

ARTICLE INFO

Keywords: Flood characteristic Urban development pattern Driving factor CaMa-flood model

ABSTRACT

Urban expansion can influence flooding by altering impervious area, surface runoff and the distribution of population. While the impact of urban development on flood hazards has been widely studied, the variation in flood characteristics in the context of urban development patterns remain insufficiently explored. This study analyzed flood characteristics and driving factors across 49 study units within the Pearl River Basin from 1998 to 2022. Using the VIC and CaMa-Flood models, we simulated river flood depth and captured inundation map. Nearly 2 % of built-up area suffer flood inundation, and by comparing inundated area without flood protection, there is around 88 % reduction in inundated area with 100-year flood protection level. Urban development patterns were identified by population and built-up area, then study units were grouped into four distinct types combined effects of flood hazard levels and urban development: (i) expanding units with hazard-improved, (ii) expanding units with hazard-unimproved, (iii) non-expanding units with hazard-improved, and (iv) non-expanding units with hazard-unimproved. Four driving factors are identified by Kolmogorov-Smirnov tests, including vegetation coverage, elevation, distance to nearest drainage and soil permeability, which significantly influence flood hazard. This study presents a novel framework for assessing flood hazards by integrating urban development heterogeneity. Results would contribute to future urban planning and enhancing flood resilience.

1. Introduction

Flooding is among the most frequent and devastating natural disasters (Kousky, 2014), casting great flood hazard on cities worldwide (Rentschler et al., 2023). Flood hazard is considered as the frequency and magnitude of flood events (Tellman et al., 2021), and results from a complex interplay of factors (Merz et al., 2021). These factors include riverine inundation, exposure, vulnerability (e.g., disadvantaged communities, inadequate infrastructure, and outdated urban planning), and urban resilience (the capacity to recover from disasters) (Kron, 2005; Laidlaw and Percival, 2024). Therefore, to identify and mitigate flood hazard, extensive researches have been conducted on the relationship between flooding and local natural and social conditions. For instance, Kumar and Acharya (2016) assessed flood hazard in Kashmir Valley

considering vegetation coverage (NDVI) change. Devitt et al. (2023) conducted a global analysis of the sensitivity of inundated areas and population exposure. Fujiki et al. (2024) explored flooding and inequality in response to poverty in France. Sohn et al. (2020) studied the effect of impervious surfaces on surface runoff and urban flooding in Texas.

Considering that impervious surface growth is accompanied by urban expansion (Shahtahmassebi et al., 2016), there exists correlation between urban development patterns and flood hazards (Idowu and Zhou, 2023). Urban development patterns have been widely discussed, aiming to comprehend regional characteristics. Generally, urban expansion results in increased impervious surfaces and higher population density (Arcaute et al., 2015; Shahfahad et al., 2021), while urban shrinkage is associated with population decline (Alves et al., 2016; Jin

https://doi.org/10.1016/j.indic.2025.100955

^{*} Corresponding author. School of Geography and Planning, Sun Yat-Sen University & Southern Marine Science and Engineering Guangdong Laboratory (Zhuhai), Zhuhai, 519000, China.

E-mail addresses: zhongm37@mail.sysu.edu.cn (M. Zhong), chentlin6@mail2.sysu.edu.cn (T. Chen), zhuol@cardiff.ac.uk (L. Zhuo), zeqiang.wang@bristol.ac.uk (Z. Wang), lingf@whigg.ac.cn (F. Ling), d.han@bristol.ac.uk (D. Han).

et al., 2024). By contrast, Sun et al. (2024) divided global urban expansion into five types in terms of population and density change. Li et al. (2022) categorized global cities into nine types by considering built-up land. Song et al. (2021) classified Chinese cities into three types: sustained shrinkage, transitional shrinkage and sustained growth by calculating population density. Therefore, flood characteristic could differ in cities because of various urban land expansion and population distribution patterns. However, much less is known regarding the difference of flood hazard under different urban development patterns, and potential factors that leads to the difference. This may undermine strengthening urban resilience against floods, due to lack of sufficient understanding of regional development, especially for the cities suffering shrinkage.

Generally, expanding cities experience expansion in impervious area and reduction in infiltration capacity, which exacerbates local flooding (Ebert et al., 2009). Shrinkage cities suffer more flood risk and socioeconomic vulnerability (Kim et al., 2025). Suburbs from Beijing in China face great increase in submerged area in the future (Jia et al., 2024). However, due to the variant development patterns among cities and regional differences within a city (Copus, 2001), there is limited understanding of the difference of flood characteristics under divergent urban development patterns.

To bridge this research gap, here we study flood hazard and urban expansion in some administrative regions within the Pearl River Basin in

China (Zhang et al., 2012). Flood hazard is assessed by calculating inundated area using hydrologic models, while urban development patterns is identified using population and built-up land data. Then flood hazard and urban development patterns are combined together to get different types of regions and unveil their divergences. The driving factors, which are sensitive to the divergence, are extracted out by analyzing flood hazard among divergent regions. Finally, suggestions are summarized to help reduce inundated area and mitigate flood hazard for regions under divergent development patterns. The findings are expected to provide actionable insights to urban planners and policy makers, hoping to enhance urban flood resilience, inform adaptive planning strategies, and promote sustainable development.

2. Study area and datasets

2.1. Study area

The Pearl River Basin, a critical region in southern China, encompasses major metropolitan areas, like Guangzhou and Shenzhen. This basin comprises the Xijiang, Beijiang, and Dongjiang watersheds, and the Pearl River Delta (Pearl River Water Resources Commission of the Ministry of Water Resources, 2015). In Fig. 1, the study units are the administrative regions through which the main river and primary tributaries flow. Finally, the study area includes 49 study units across 13

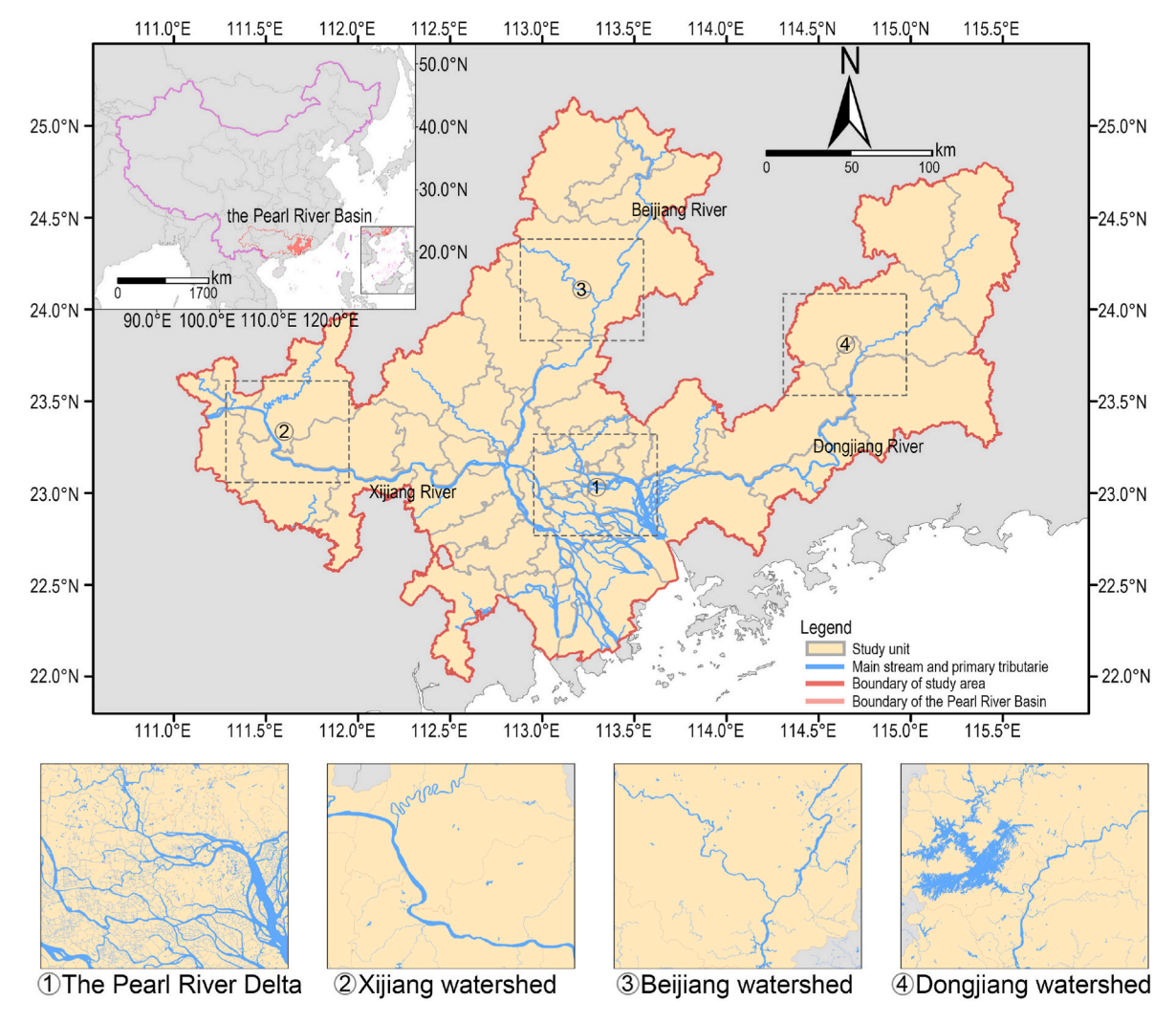


Fig. 1. The distribution of study units, and main streams and primary tributaries. Bold red line circles the study area, grey line separate study area into 49 study units, and red line denote the Pearl River Basin. Blue line indicates main streams and primary tributaries. The region denoting (1) the Pearl River Delta, (2) Xijiang, (3) Beijiang and (4) Dongjiang watersheds are boxed out respectively.

cities (attached in Supplementary Table 1).

2.2. Data source

Flood characteristic is analyzed supported by CN05.1 dataset. CN05.1 derives from China Meteorological Data Service Centre (htt ps://data.cma.cn/) (Wu and Gao, 2013), and is interpolated from data collected at over 2400 Chinese meteorological stations (Wu et al., 2017). With a spatial resolution of $0.25^{\circ} \times 0.25^{\circ}$, the dataset covers the period from 1961 to 2022 for entire China and is widely used for validating high-resolution climate models. Merit Hydro is a global datasets with a spatial resolution of 15-arcsec (Yamazaki et al., 2011), which includes flow direction and river channel width (https://hydro.iis.u-tokyo.ac.jp/). It can be used for estimating river channel information and flood simulation.

Urban development pattern is identified using population and built-up land data. For details, population data is sourced from the China Economic and Social Big Data Platform (https://data.cnki.net/) (Zhang et al., 2022), covering the whole study period. Built-up area data is derived from China Land Cover Dataset (CLCD) (Zhang et al., 2022; Zou et al., 2022), which demonstrates strong spatio-temporal consistency with the high resolution at 30 m from 1985 to 2022.

Factors (Table 1) across 49 study units consider local socio-economic and natural conditions, which could potentially influence flood hazard. For details, the growth of GDP (global domestic product) can induce decrease in floods by improving production efficiency (Ceesay, 2020). Intense population in flood-prone area increase potential damage when extreme flood event occurs (Ferdous et al., 2020). NDVI (vegetation coverage) is a significant predictor to explain variation in runoff and impact on flooding (Kim et al., 2017). High-altitude regions are considered to be less exposed to storms and flooding since these disasters mainly hit coastal areas or villages around rivers (Ronco et al., 2023). Precipitation, wind speed and temperature have been verified to be related to runoff generation (Liang et al., 1994), which finally leads to flooding. HAND (the height above the nearest drainage) is a good indicator of hydrology-relevant topography (Jiang et al., 2023), and widely discussed for flood risk management. The expansion of urban land and variation of soil property can impact surface runoff, which then influences flood occurrence (Ma et al., 2024). Besides, flat to gentle slope makes runoff get stored and dispose out gradually, so low gradient slopes at lower reaches are highly vulnerable to flood occurrence (Ramesh and Iqbal, 2022). R-B (Richards-Baker flashiness index) is used to reflect the frequency and rapidity of short-time changes in streamflow (Baker et al., 2004), and analyze flood risk perception (Knighton et al., 2021).

3. Methods

This study analyzes flood characteristics and driving factors under urban development patterns through a four-step methodological framework. The proposed method first utilizes VIC and CaMa-Flood models to generate simulated inundated area distribution. The inundated area is then used to assess flood characteristics using Mann-Kendall trend tests. Thereafter, urban development pattern is evaluated by quantifying changes in population and population density. Finally, by combining flood characteristics with urban development patterns, the study units are classified into various types. Kolmogorov-Smirnov tests are conducted to identify driving factors across different types of study units. The difference of urban development pattern and applicability of driving factors are carefully analyzed to mitigate flood hazard.

3.1. Flood inundation simulation

The VIC (Variable Infiltration Capacity) and CaMa-Flood (Catchment-based Macro-scale Floodplain) models are coupled together to perform flood simulations. The VIC model is a macroscale, distributed hydrological model developed by the University of Washington (Liang et al., 1994). It has been widely used for river runoff simulation. The CaMa-Flood is a global river model (Yamazaki et al., 2011), which incorporates floodplain dynamics through sub-grid parameterization and has been extensively used to generate flood inundation maps.

In this study, the VIC model is first used to simulate daily runoff in the study area. The model inputs data include daily minimum temperature, maximum temperature, precipitation, and wind speed from CN05.1 dataset. The generated runoff data is then input into the CaMa-Flood model, which generates river flood depth. The soil and vegetation parameters required for VIC model were consistent with the previous study (Zhong et al., 2023).

Flood depth is first computed at 1 arcmin (nearly 1800 m at the equator) and then downscaled onto a 15-arcsec (approximately 450 m) high-resolution digital elevation model (DEM) (Dottori et al., 2018). By analyzing the spatial distribution of the simulated inundation depth in built-up area, simulated inundated area and inundation ratio are calculated. The maximum inundated area within a year is then calculated, which is considered as annual flood inundation area. The inundation ratio is the value of the simulated inundated area divided by the built-up area.

Different locations differ in natural conditions, urban sizes, and flood protection standards (Ward et al., 2017; Dottori et al., 2018). The levees in the cities located in study area have reached the flood protection level of at least 100 - year return period (https://dara.gd.gov.cn/zwgk/z

Table 1The potential factors.

Factor	Definition	Unit	Source
GDP	GDP per capita in study unit	RMB/ person	China Economic and Social Big Data Platform (https://data.cnki.net/)
Population density	The density of the population	person/ km²	
NDVI	Annual vegetation coverage in built-up area	-	Institute of Geographic Sciences and Natural Resource Research, CAS (http://english.igsnrr.cas.cn/)
Elevation	The average elevation of built-up area	m	Geospatial Data Cloud (https://www.gscloud.cn/)
Precipitation	Annual average precipitation	mm/day	Climate Change Research Center (https://data.cma.cn/)
Wind speed	Annual average wind speed	m/s	
Temperature	Annual average temperature	°C	
HAND	The height above the nearest drainage in built-up area	m	Merit Hydro (https://hydro.iis.u-tokyo.ac.jp/)
Land cover change	The growth rate of built-up area	-	Annual China Land Cover (https://essd.copernicus.org/articles/13/3907/2021/)
Soil permeability	The ease with water penetrates through the soil in	_	Geographic Data Sharing Infrastructure, global resources data cloud (http://www.
	built-up area		gis5g.com/)
Terrain slope	The degree of steepness in built-up area	0	SRTM product (https://earthexplorer.usgs.gov/)
R-B	Frequency and rapidity of the short-term changes in streamflow	-	The water resources bulletin (https://www.pearlwater.gov.cn/zwgkcs/lygb/szygb/)

cwj/content/post_3577642.html). Besides, Dottori et al. (2018) used present-day flood protection levels obtained from FLOPROS to calculate present and future flood risk, in which the flood protection levels was set as a return period of 100 years in China. Therefore, our work is conducted in the context of 100-year flood protection standard by considering the height of the levee (attached in Supplementary Note 4).

3.2. Classification of urban development pattern

Population and built-up area data are utilized to classify urban development patterns, following the approach of Sun et al. (2024). Specifically, built-up area is considered difficult to reduce because of the limited arable land reclamation (Wang et al., 2020). The threshold for the change of population (UPD_{dt}) and population density (P_{dt}) are both set at 1 % (Oswalt et al., 2006). The relevant formulas are as follows:

$$UPD_t = \frac{P_t}{B_t} \tag{1}$$

$$P_{dt} = (P_{t+n} - P_t) \tag{2}$$

$$UPD_{dt} = (UPD_{t+n} - UPD_t)$$
(3)

where P_t is the population, B_t is the area of built-up area, UPD_t is the population density, t represents the first reference year, and t+n represents the last reference year

The urban development patterns of study units are categorized into two types: expanding units, characterized by an increasing population or built-up area, and non-expanding units, characterized by a constant or decreasing trend in population or built-up area. Following the approach of Sun et al. (2024), a unit is classified as an expanding unit when any of the following conditions hold: $UPD_{dt} > 0$ %, $UPD_{dt} = 0$ % & $P_{dt} > 0$ %, or $UPD_{dt} < 0$ % & $P_{dt} \geq 0$ %. Conversely, a unit is classified as a non-expanding unit when $UPD_{dt} = 0$ % & $P_{dt} = 0$ % or $UPD_{dt} < 0$ % & $P_{dt} < 0$ % &

4. Results

4.1. Identification of flood characteristic

Using the method described in Section 3.1, Figs. 3 and 4 illustrate the

spatial distribution of simulated inundated areas and flood characteristics from 1998 to 2022, considering 100-year flood protection level. The simulated inundated area is validated with the support of flood extent from Global Flood Database (Tellman et al., 2021) (attached in Supplementary Note 2). By comparing simulated inundated area with 100-year flood protection level to no flood protection (Fig. 2b), there is approximately 88 % reduction in inundated area. This highlights the significant role of flood control facilities in river flood prevention. For the entire study area (Fig. 2a), the built-up area expanded nearly three times from 1998 to 2022. Simulated inundation ratio (Fig. 2a) began to rise in 1998, reached its peak (2.1 %) in 2015, and then gradually decreased, maintaining at around 2.0 %. This can be explained that the newly-developed urban land was further to the rivers than the original urban land after 2015, and the latter was already located near the river (Jiang et al., 2023). For the Pearl River Delta (Fig. 3a), the built-up area experienced significant expansion over the 25-year period, accompanied by an increase in simulated inundated area. In contrast, the Xijiang and Beijiang watersheds (Fig. 3b and c) exhibited relatively slower expansion of both built-up and inundated areas, which were predominantly distributed along river banks. In Dongjiang watershed (Fig. 3d), the built-up area expanded considerably from its original extent, while the simulated inundated area showed only marginal growth.

Finally, by using the Mann-Kendall trend test (Fattah et al., 2024), the trend of the simulated inundation ratio in each study unit was identified, including three types: increasing, decreasing trend, and no trend. The decreasing type is considered the units with hazard-improved, indicating the mitigation in flood hazard. Conversely, the increasing and no trend types are classified into units with hazard-unimproved, suggesting the suffering constant or worsening flooding in these regions. The distribution of study units with different flood characteristics is presented in Fig. 2c. Of the total study units, 31 are classified as hazard-improved units, while 18 are categorized as hazard-unimproved units.

4.2. Identification of urban development pattern

The urban development patterns of the study units from 1998 to 2022 are explored in Fig. 4a, revealing that all study units are identified as expanding units. During this period, all the study units experienced rapid development, marked by increasing populations and built-up

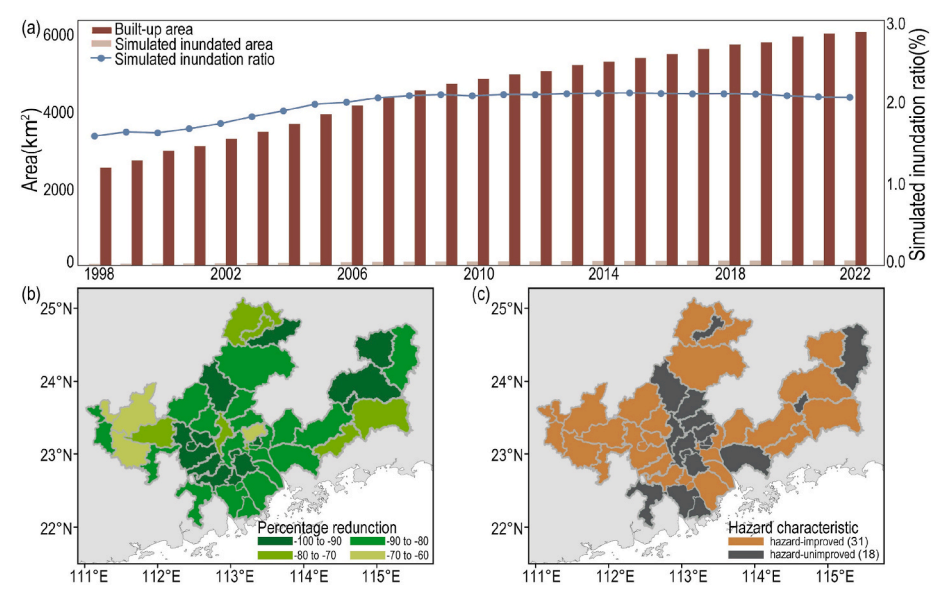


Fig. 2. a The temporal change of built-up area (sienna bar), simulated inundated area (wheat bar), and annually simulated inundation ratio (blue points) from 1998 to 2022; b Percentage reduction in average simulated inundated area with 100-year flood protection level compared to no flood protection. Green bands indicate percentage reduction respectively; c Spatial distribution of units with hazard-improved (chocolate), and units with hazard-unimproved (grey).

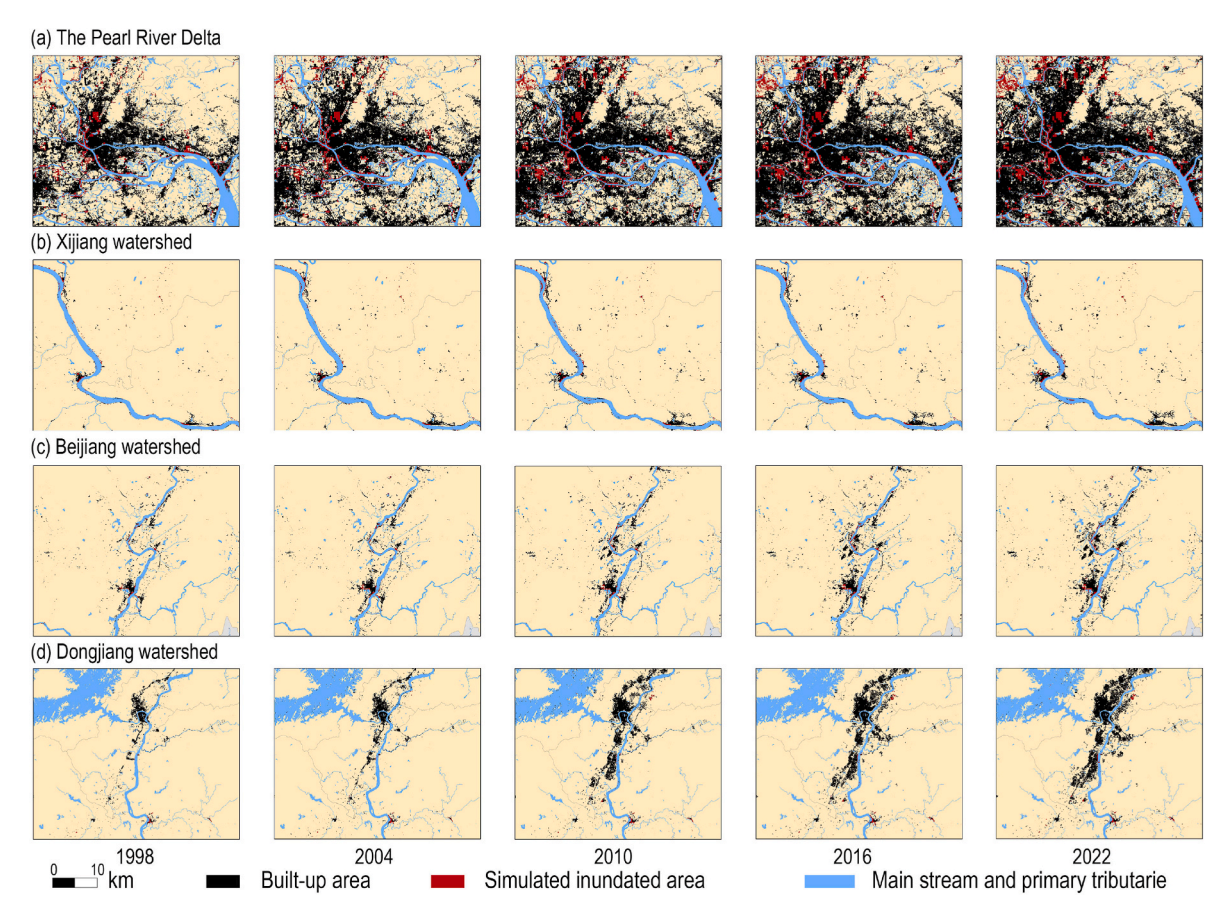


Fig. 3. The spatial distribution of built-up area (black) and simulated inundated area (dark red) within a the Pearl River Delta, b Xijiang, c Beijiang and d Dongjiang watersheds, taking five years for example. Blue line indicates main streams and primary tributaries.

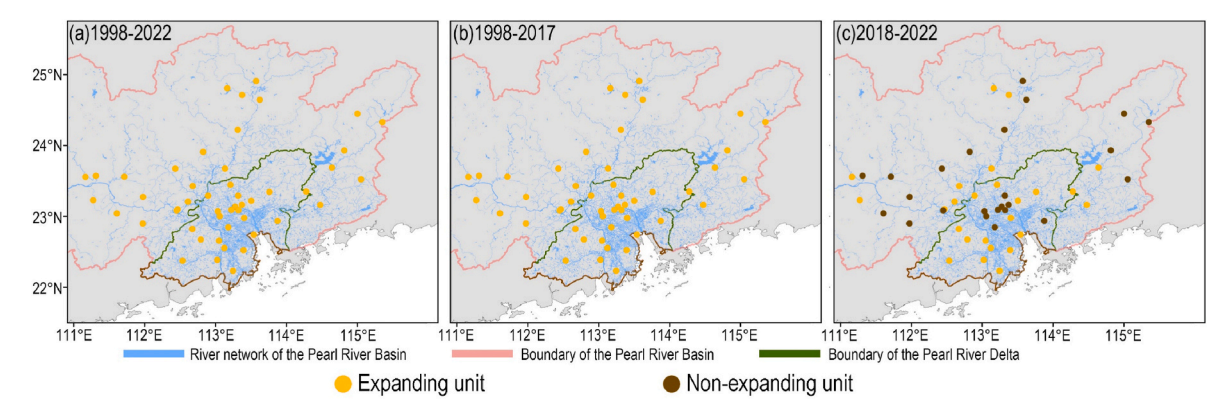


Fig. 4. Identified urban development patterns from a 1998 to 2022, b 1998 to 2017 and c 2018 to 2022. Yellow scatters represent expanding units, while brown ones represent non-expanding units.

areas. Considering 2017 marks the high-quality urban advancement in China and the significant regional disparities persist among cities from 2017 to 2021 (Qin and Qin, 2025), we further divided the study period into two phases: 1998–2017 and 2018–2022. By segmenting the study period, it can be more clearly observed that how urban development patterns evolved.

From 1998 to 2017 (Fig. 4b), none of the study units were non-expanding units, a trend consistent with the entire study period. However, from 2018 to 2022 (Fig. 4c), the number of non-expanding units increased significantly, rising from zero to 24, highlighting a shift in urban development patterns during this phase. In contrast, the number of expanding units remained at 25, nearly equal to the number of non-

expanding units. Notably, most of the expanding units are located within the Pearl River Delta.

4.3. Combining analysis between flood characteristics and urban development pattern

To further explore the variation of flood characteristic under divergent urban development pattern, the study units were further classified into four types, as shown in Fig. 5b, as expanding units with hazard-improved (17 of 49 units), expanding units with hazard-unimproved (8 units), non-expanding units with hazard-improved (14 units), and non-expanding units with hazard-unimproved (10 units) (attached in

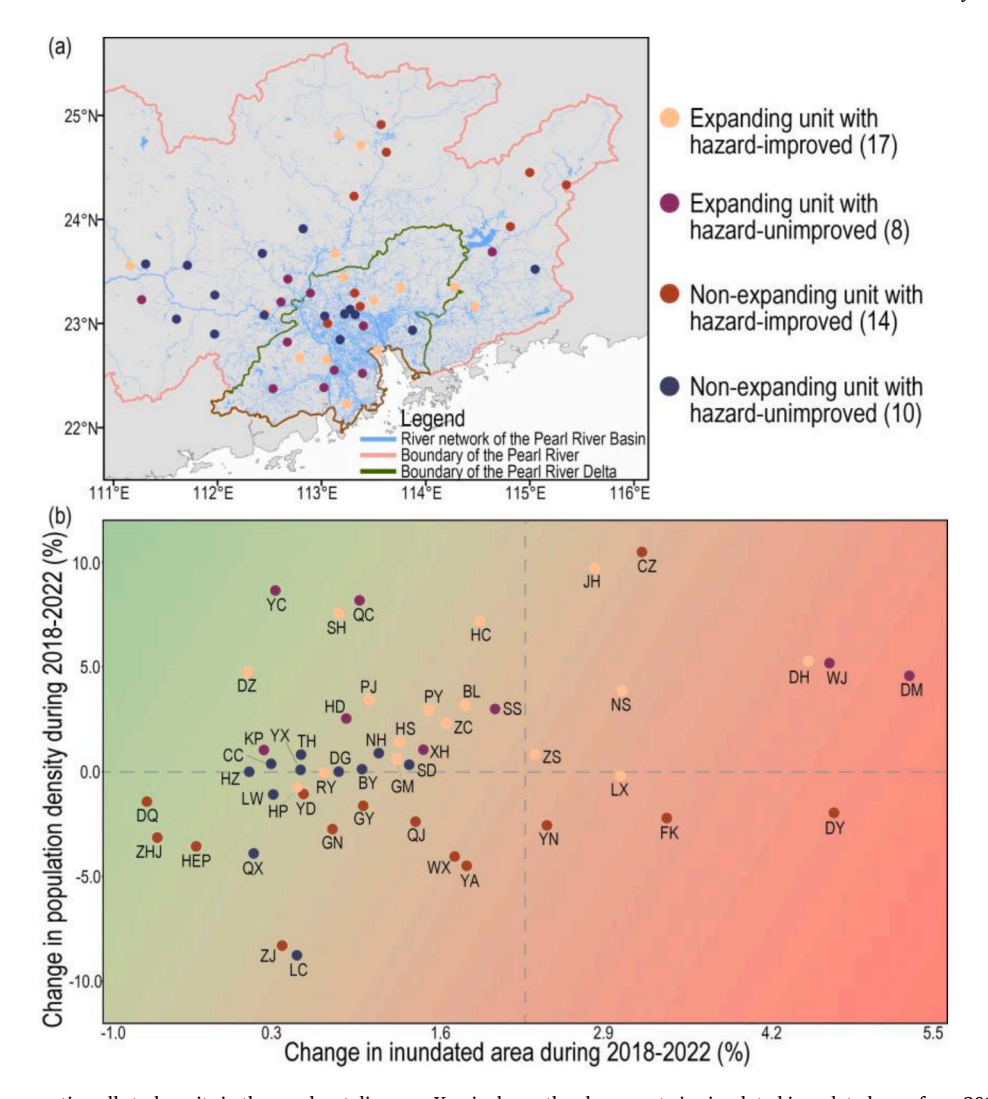


Fig. 5. a Scatter plots representing all study units in the quadrant diagram. X-axis shows the change rate in simulated inundated area from 2018 to 2022, while Y-axis shows the change rate in population density from 2018 to 2022; b Spatial distribution of the identified four types of study units: expanding units with hazard-improved (orange), expanding units with hazard-unimproved (magenta), non-expanding units with hazard-improved (maroon), and non-expanding units with hazard-unimproved (dark blue).

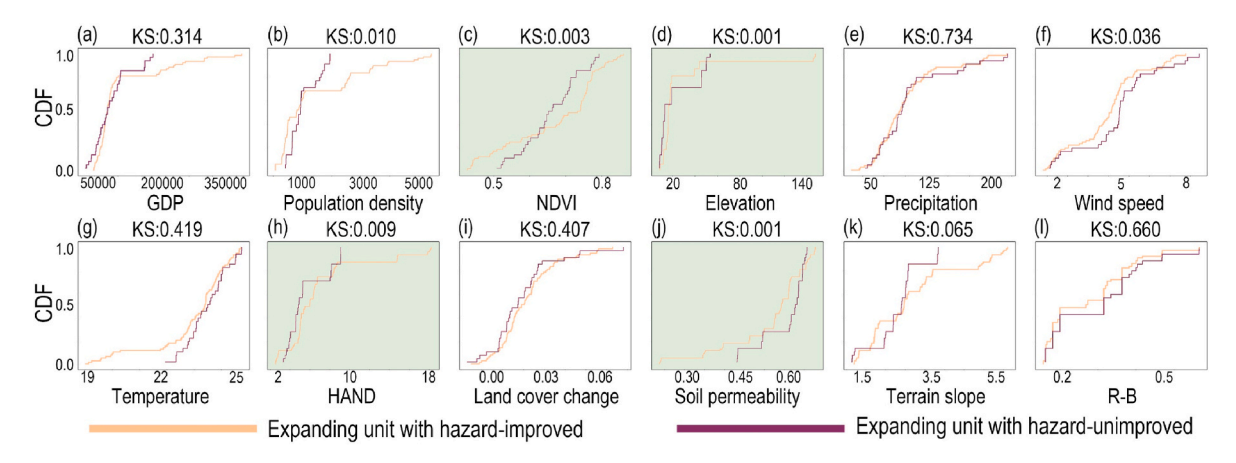


Fig. 6. Cumulative distribution figures (CDF) for expanding units with hazard-improved (orange) and expanding unit with hazard-unimproved (magenta) about a GDP, b population density, c NDVI, d elevation, e precipitation, f wind speed, g temperature, h HAND, i land cover change, j soil permeability, k terrain slope and l R-B. KS indicates two-sample KS-test P value. Green shading indicates sensitivity at $\alpha < 0.01$.

Supplementary Table 2).

To explore the attributes of the four types of study units, a point graph (Fig. 5a) was created to show the change rates in population density and simulated inundated area from 2018 to 2022, and it was divided into four quadrants. Specifically, when the change rate in population density exceeds 0, the units are classified as expanding units; otherwise, they are non-expanding. This indicates a strong correlation between city expansion and population density increase. When the change rate in inundated area is below 0.0 %, the units are categorized as hazard-improved. The three units in the fourth quadrant are all non-expanding units with hazard-improved, resulting from decreasing city size and decreasing flood inundation hazard. 27 units, with change rates in inundated area ranging between 0.3 % and 1.6 %, exhibit mixed trends in city size and include all four types of study units.

4.4. Analysis of driving factors

The Kolmogorov-Smirnov test (Ohunakin et al., 2024) was conducted to determine driving factors between hazard-improved and hazard-unimproved units, considering expanding and non-expanding types separately. For the expanding units (Fig. 6), the driving factors with a P-value below 0.01 include NDVI, elevation, HAND and soil permeability. Specifically, Fig. 6c shows that about 70 % of units with hazard-improved have greater NDVI than those with hazardunimproved. This suggests that enhancing vegetation coverage could help transform units into hazard-improved ones. In Fig. 6d, there are distinct differences in elevation between the two types of units. As the elevation is over 70 m or below 30 m, built-up area in units with hazardimproved is higher. This indicates the influence of elevation in built-up area in mitigating flood hazard. Regarding HAND (Fig. 6h), the value in hazard-improved units are generally higher, supporting the consensus that keeping distance to rivers reduces flood risk (Njoku et al., 2020). In Fig. 6j, the orange line representing expanding units with hazard-unimproved lies below the magenta line, indicating that these units tend to have higher soil permeability. This can be explained that places with high natural soil permeability suffered less water retention and were more suitable for human living and urban expansion (Yu et al., 2019). However, large-scale expansion of impervious surface area conversely leads to increase in surface runoff and exacerbates flood hazard (Du et al., 2015). For other factors, the lines for both types of units tend to overlap with P-values greater than 0.01, suggesting that these factors are not significant driving forces.

Similar to the expanding units in Fig. 6, non-expanding units (Fig. 7) also show that NDVI, elevation, HAND and soil permeability are driving factors. Units with hazard-improved tend to have denser vegetation coverage, higher elevation, further distance to the nearest river and

relatively lower soil permeability compared to those with hazard-unimproved. Besides. GDP, population density, temperature, land cover change and terrain slope are driving factors with P-value below 0.01. Considering the geographical location of units with hazard-unimproved (Fig. 7b), the sensitivity of these factors is likely related to the distribution of NDVI, elevation, HAND and soil permeability. A linear correlation analysis (Fig. 8) was then conducted to explain this relationship.

The normalization is conducted for factors. As can be seen from Fig. 8, units with lower vegetation coverage, tend to have higher population density, fatter terrain, higher temperature and higher GDP. These units are mostly distributed in the Pearl River Delta (Fig. 5b), which is a region with subdued topography, developed economy and high carbon emission (Xu et al., 2018). It's noteworthy that carbon emission is related to heat-island effect (Wang et al., 2020), causing an increase in temperature. Regarding elevation and HAND, units with higher elevation and further distance to nearest rivers, tend to have lower population density, steeper terrain, lower temperature and lower GDP. As for soil permeability, there is no direct linear correlation in GDP, population density and built-up area change. Besides, units showing strong soil permeability are following higher temperature and fatter terrain, and they are mainly situated at the estuary (Fig. 5b). This further suggesting the influence of soil permeability in flood hazard mitigating (Figs. 6j and 7j). Moreover, distinctly strong linear correlation exists among NDVI, and elevation, HAND and soil permeability.

5. Discussion

5.1. The differences of urban development patterns

According to the results of urban development patterns (Fig. 4), all the units are expanding units from 1998 to 2017. However, between 2018 and 2022, 24 non-expanding units emerged. These differences in development patterns are attributed to variations in urban development orientation, geographical location, and population dynamics, which create competition among units.

The 49 study units in this work are located within 13 cities (see Supplementary Table 1). According to the Outline Development Plan for the Guangdong-Hong Kong-Macao Greater Bay Area released by the Chinese government (https://www.gov.cn/zhengce/2019-02/18/content_536659 3.htm#1), 13 cities are classified into three categories: core cities, node cities, and nearby cities. Specifically, Guangzhou is identified as the core city, playing a leading role in the development of the Greater Bay Area and serving as an integrated transport hub. The node cities—Foshan, Dongguan, Zhongshan, Zhuhai, Huizhou, and Jiangmen, demonstrate strong interaction and cooperation with the core city. The nearby cities—Qingyuan, Shaoguan,

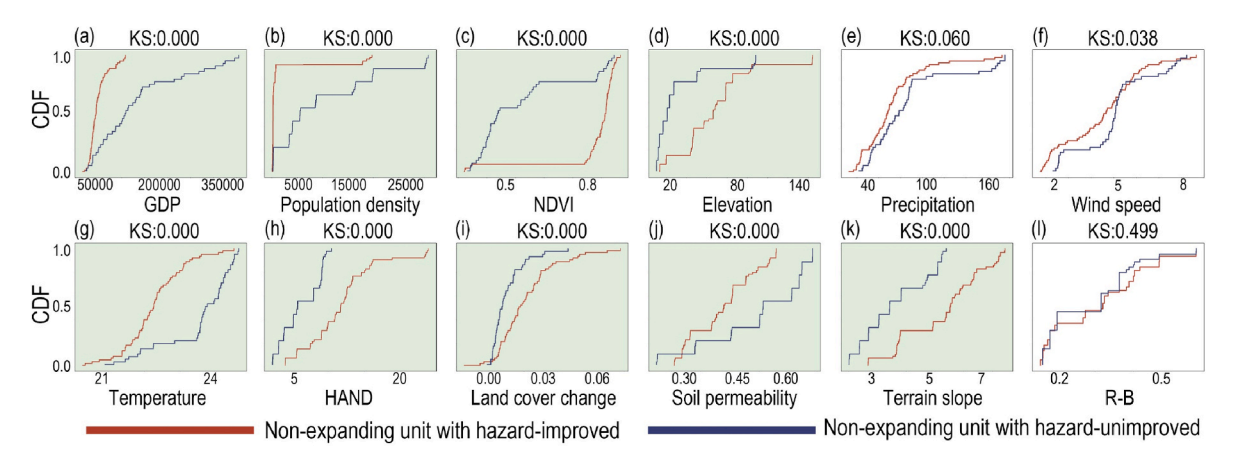


Fig. 7. Cumulative distribution figures (CDF) for non-expanding units with hazard-improved (maroon) and non-expanding unit with hazard-unimproved (dark blue) about a GDP, b population density, c NDVI, d elevation, e precipitation, f wind speed, g temperature, h HAND, i land cover change, j soil permeability, k terrain slope and 1 R-B. KS indicates two-sample KS-test P value. Green shading indicates sensitivity at $\alpha < 0.01$.

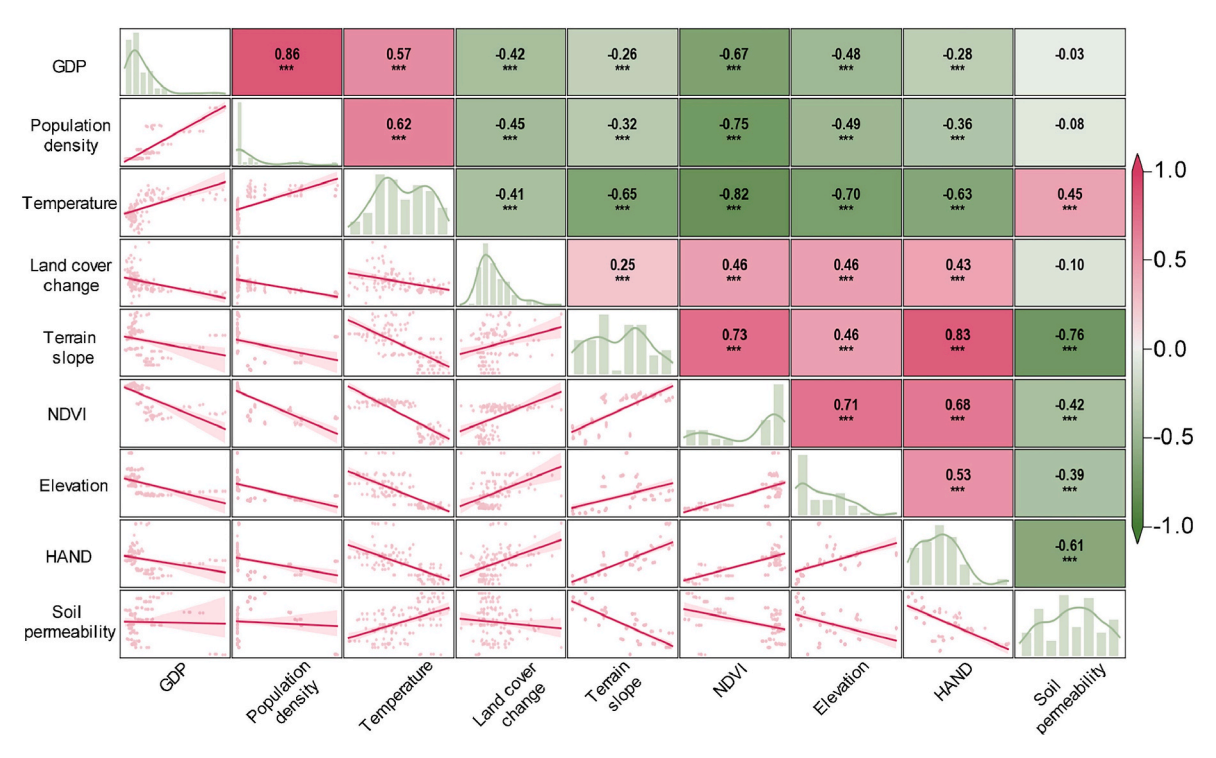


Fig. 8. Heat maps (above the diagonal), histograms (diagonal) and scatter plots (below the diagonal) for driving factors in non-expanding units. Heat maps suggest the correlation coefficient between two driving factors. The color bar indicates Pearson correlation values, ranging from -1.0 to 1.0. "*", "**", and "***" denotes P value below 0.1, 0.05 and 0.01 respectively. Histograms show the distribution of driving factors with the Kernel density estimation curves. Scatter plots show the relationship between two driving factors with the fitting line and 95 % confidence interval.

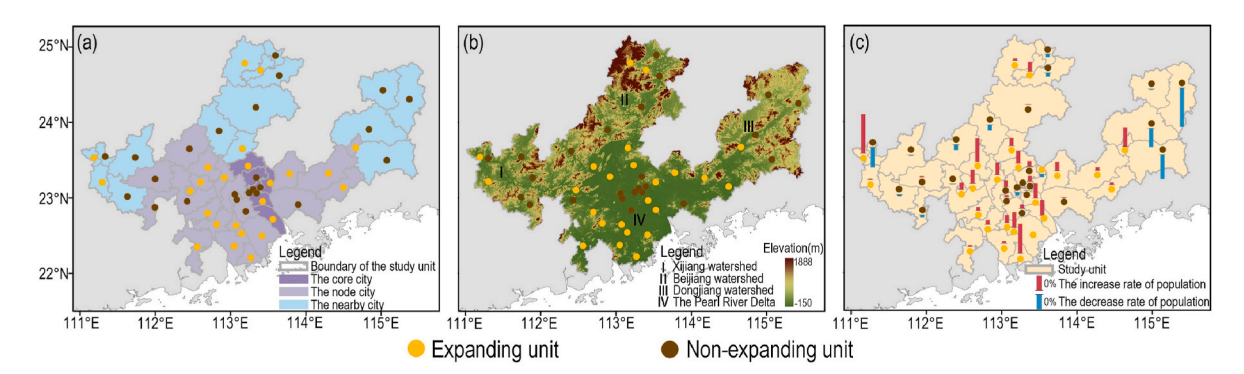


Fig. 9. an Urban development orientations of 49 study units with two types of urban development patterns; purple area represents the core city, light purple area represents the node city, and light blue represents the nearby city; **b** Geographical location of 49 study units; I-IV means Xijiang watershed, Beijinag watershed, Dongjinag watershed and the Pearl River Delta separately (elevation is showed in the color bar); **c** Population dynamics of those 49 units (red bar represents the increase rate of population from 2018 to 2022, while blue bar represents the decrease rate of population from 2018 to 2022).

Wuzhou, Yunfu, and Heyuan, are located adjacent to the Greater Bay Area and are influenced by the radiation effect of the node cities. As shown in Fig. 9a, among the units in the nearby cities, 11 are non-expanding and 5 are expanding. This suggests that these units face disadvantages in regional development, with limited opportunities for growth. In the node cities, the number of expanding units (16) exceeds that of non-expanding units (8), indicating greater development opportunities and the potential for expansion through cooperation with the core city. In contrast, the core city units show a nearly balanced distribution, with 4 expanding and 5 non-expanding units. This pattern indicates that differences in urban development orientations influence the variations in development patterns across the region.

In terms of geographical location, the study units are situated within the Xijiang, Beijiang, and Dongjiang watersheds, and the Pearl River Delta (Fig. 9b). The elevation map reveals that the Pearl River Delta has lower terrain compared to the other three watersheds. This, characterized by flat terrain and its proximity to the estuary, is more conducive to

economic development and population concentration. Consequently, the units in the Pearl River Delta (Fig. 4c) are predominantly expanding units. In contrast, the three watersheds with higher terrain are largely covered by mountainous and hilly areas, which hinder local economic development and expansion of built-up areas. Finally, there are more non-expanding units than expanding ones in these areas. This suggests that variations in geographical location significantly influence urban development patterns.

Differences in population dynamics also play a significant role in shaping variations in urban development patterns. As shown in Fig. 9c, most non-expanding units have experienced population decline, while the majority of expanding units have seen an increase in population. This suggests that population growth tends to drive urban expansion in the study area.

5.2. The applicability of driving factors

Regardless of the type of urban development patterns, NDVI, elevation, HAND and soil permeability have a significant impact on flood hazard (Figs. 6 and 7). Specifically, non-expanding units with hazard-unimproved (NU in Fig. 10a) have considerably lower vegetation coverage than the other three types of units. This is primarily because this type of units is distributed in highly developed region (Fig. 5b). NDVI of expanding units with hazard-improved (EI in Fig. 10a) is slightly higher than that of expanding units with hazard-unimproved (EU in Fig. 10a). Therefore, for expanding units, it is essential to increase Greenland. For non-expanding units, it is advised to enhance vegetation coverage in urban land, like following nature-based solution (Opperman and Galloway, 2022)

In terms of elevation and HAND (Fig. 10b and c), non-expanding units with hazard-improved are situated at higher elevations with further distance to rivers than the other units. Besides, elevation and HAND in expanding units with hazard-improved are relatively higher than expanding units with hazard-unimproved. This suggests that higher elevation and further distance to nearest drainage can help improve flood hazard. However, expanding units (EI and EU in Fig. 10b and c) are primarily located in the Pearl River Delta (Fig. 4c), which is significantly lower in elevation and nearer to rivers compared to non-expanding units (NI and NU in Fig. 10b and c). This makes the expanding units more vulnerable to flood hazard. Therefore, for expanding units, urban planning should prioritize the development of new areas on higher ground and maintain distance from the nearest drainage, aiming to reduce flood exposure. For non-expanding units, given the constraints on expanding built-up areas, the focus should be on strengthening flood control infrastructure, including dams and levees.

For soil permeability in expanding units (Fig. 10d), the overall levels of permeability across the four categories are similar. However, expanding units with hazard-unimproved have slightly higher permeability than expanding units with hazard-improved, and non-expanding units with hazard-unimproved have obviously higher permeability than those with hazard-improved. This refers to the results in Figs. 6j and 7j, and soil permeability is natural property and calculated without considering impervious surface. Therefore, regardless of urban development patterns, units should utilize soil permeability and other permeable materials to improve the permeability of urban land. For example, constructing a "sponge city" in flood susceptible areas (Aksoy et al., 2025).

5.3. Limitation

Further research is needed to focus on the detailed mechanism of NDVI and soil permeability, such as the possible existence of mediating variables. This could help understand how vegetation coverage affects flooding in built-up area at a deeper level. Besides, our work mainly concentrated on flood hazard. In the future research, flood risk, which includes flood hazard, exposure and vulnerability, is needed to comprehensively analyze within the study area.

6. Conclusion

This study aimed to explore characteristics and drivers of flood hazard under different urban development patterns across 49 study units within the Pearl River Basin. Using VIC and CaMa-Flood models, the flood characteristics were identified in the context of 100-year flood protection level. Nearly 2 % of the built-up area suffer flood inundation, and by comparing inundated area without flood protection, there is around 88 % reduction in inundated area with 100-year flood protection level. Besides, using Mann-Kendall trend test, flood characteristic can be classified into hazard-improved and hazard-unimproved.

Urban development patterns were identified by population and builtup area, which includes expanding and non-expanding types. This divergence is related to development orientation, geographical location, and population dynamics. Then study units were grouped into four distinct types combined effects of flood hazard levels and urban development: (i) expanding units with hazard-improved, (ii) expanding units with hazard-unimproved, (iii) non-expanding units with hazardimproved, and (iv) non-expanding units with hazard-unimproved.

Based on the results of Kolmogorov-Smirnov tests, this study identified four driving factors that significantly influence flood characteristics, including vegetation coverage, elevation, distance to nearest drainage and soil permeability. Considering the applicability, hazard-improved units have relatively lager vegetation coverage, higher elevation and further distance to rivers. Moreover, it is necessary to improve urban surface permeability, which helps reduce surface runoff and mitigate flood hazard.

In conclusion, our work is to draw practical conclusions to reduce flood hazards and provide actionable recommendations for policy-makers. From an urban planning perspective, newly developed areas should be carefully planned and situated in higher-elevation zones and keep safe distance to rivers. Proper planning of green land and utilization of soil permeability are also essential to mitigate flood hazard.

CRediT authorship contribution statement

Ming Zhong: Writing – original draft, Validation, Project administration, Methodology, Formal analysis, Data curation, Conceptualization. Tailin Chen: Writing – original draft, Software, Methodology, Investigation, Formal analysis, Data curation. Lu Zhuo: Writing – review & editing, Validation, Resources, Formal analysis, Data curation. Zeqiang Wang: Writing – review & editing, Validation, Investigation, Data curation. Feng Ling: Writing – review & editing, Validation,

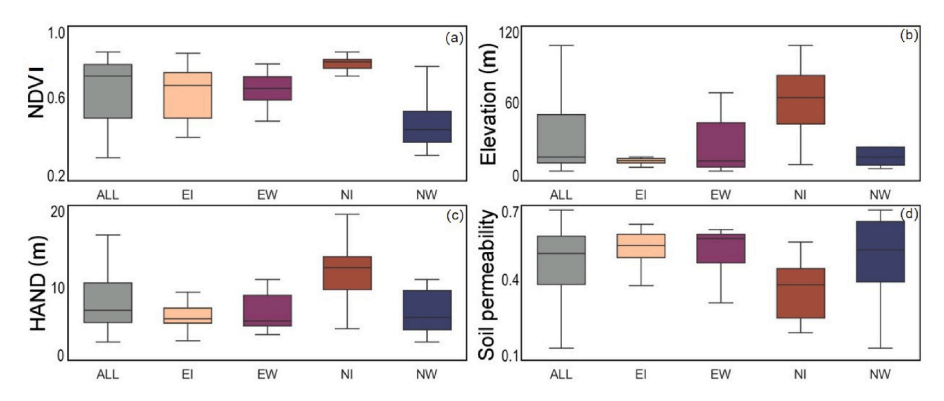


Fig. 10. Boxplots of a NDVI, b elevation, c HAND, and d soil permeability for four types of study units: expanding units with hazard-improved (EI; orange), expanding units with hazard-unimproved (EU; magenta), non-expanding units with hazard-improved (NI; maroon) and non-expanding units with hazard-unimproved (NU; dark blue), and all study units (ALL; grey).

Resources, Data curation. **Dawei Han:** Writing – review & editing, Validation, Supervision, Resources, Methodology.

Acknowledgement

This work was supported by the National Natural Science Foundation of China (Grant No. 42571088).

Declaration of competing interest

The authors declare that they have no known competing financial interests or personal relationships that could have appeared to influence the work reported in this paper.

Appendix A

Supplementary documents to this article can be found online at https://doi.org/10.1016/j.indic.2025.100955.

Data availability

The data that support the findings of this study are available upon request. Restrictions may apply to the availability of data due to privacy or ethical considerations.

References

- Aksoy, O., Erken, K., Sökmen, E.D., 2025. Application of sponge city strategies in flood susceptible areas; Hatay, antakya example. Nat. Hazards 121 (4), 4781–4801. https://doi.org/10.1007/s11069-024-07001-5.
- Alves, D., Barreira, A.P., Guimarães, M.H., Panagopoulos, T., 2016. Historical trajectories of currently shrinking Portuguese cities: a typology of urban shrinkage. Cities 52, 20–29. https://doi.org/10.1016/j.cities.2015.11.008.
- Arcaute, E., Hatna, E., Ferguson, P., Youn, H., Johansson, A., Batty, M., 2015. Constructing cities, deconstructing scaling laws. J. R. Soc. Interface 12 (102), 20140745. https://doi.org/10.1098/rsif.2014.0745.
- Baker, D.B., Richards, R.P., Loftus, T.T., Kramer, J.W., 2004. A new flashiness index: characteristics and applications to midwestern Rivers and streams. J. Am. Water Resour. Assoc. 40 (2), 503–522. https://doi.org/10.1111/j.1752-1688.2004. tb01046.x.
- Ceesay, E.K., 2020. Does flood disaster lessen GDP growth? Evidence from the gambia's manufacturing and agricultural sectors. J. Petrol Environ. Biotechnol. 11 (404). https://doi.org/10.35248/2157-7463.20.11.404.
- Copus, A.K., 2001. From core-periphery to polycentric development: concepts of spatial and aspatial peripherality. Eur. Plan. Stud. 9 (4), 539–552. https://doi.org/10.1080/ 09654310120049899.
- Devitt, L., Neal, J., Coxon, G., Savage, J., Wagener, T., 2023. Flood hazard potential reveals global floodplain settlement patterns. Nat. Commun. 14 (1), 2801. https://doi.org/10.1038/s41467-023-38297-9
- Dottori, F., Szewczyk, W., Ciscar, J.C., Zhao, F., Alfieri, L., Hirabayashi, Y., Bianchi, A., Mongelli, I., Frieler, K., Betts, R.A., Feyen, L., 2018. Increased human and economic losses from river flooding with anthropogenic warming. Nat. Clim. Change 8 (9), 781–786. https://doi.org/10.1038/s41558-018-0257-z.
- Du, S., Shi, P., Van Rompaey, A., Wen, J., 2015. Quantifying the impact of impervious surface location on flood peak discharge in urban areas. Nat. Hazards 76 (3), 1457–1471. https://doi.org/10.1007/s11069-014-1463-2.
- Ebert, A., Banzhaf, E., McPhee, J., 2009. The Influence of Urban Expansion on the Flood Hazard in Santiago De Chile. Joint Urban Remote Sensing Event, pp. 1–7. https://doi.org/10.1109/URS.2009.5137601, 2009.
- Ferdous, M.R., Di Baldassarre, G., Brandimarte, L., Wesselink, A., 2020. The interplay between structural flood protection, population density, and flood mortality along the jamuna river, Bangladesh. Reg. Environ. Change 20 (1), 5. https://doi.org/ 10.1007/s10113-020-01600-1.
- Fujiki, K., Finance, O., Hirtzel, J., Enaux, C., 2024. Flooding and inequality: a multilevel analysis of exposure to floods and poverty in French cities. Appl. Geogr. 164, 103193. https://doi.org/10.1016/j.apgeog.2023.103193.
- Idowu, D., Zhou, W., 2023. Global megacities and frequent floods: correlation between urban expansion patterns and urban flood hazards. Sustainability 15 (3), 2514. https://doi.org/10.3390/su15032514.
- Jia, M., Lin, J., Dai, J., Zhang, J., 2024. Assessing future flood risks in megacity suburbs under shared socioeconomic pathways (SSPs) scenarios: a case study of beijing. Urban Clim. 58, 102208. https://doi.org/10.1016/j.uclim.2024.102208.
- Jiang, R., Lu, H., Yang, K., Chen, D., Zhou, J., Yamazaki, D., Pan, M., Li, W., Xu, N., Yang, Y., Guan, D., Tian, F., 2023. Substantial increase in future fluvial flood risk projected in China's major urban agglomerations. Commun. Earth Environ. 4 (1), 389. https://doi.org/10.1038/s43247-023-01049-0.

- Jin, Y., Zhou, G., Sun, H., Fu, H., Wu, H., Liu, Y., 2024. Regrowth or smart decline? A policy response to shrinking cities based on a resilience perspective. Sustain. Cities Soc. 108, 105431. https://doi.org/10.1016/j.scs.2024.105431.
- Kim, H.W., Kim, J.H., Li, W., Yang, P., Cao, Y., 2017. Exploring the impact of green space health on runoff reduction using NDVI. Urban For. Urban Green. 28, 81–87. https://doi.org/10.1016/j.ufug.2017.10.010.
- Kim, Y.E., Lee, J., Kim, H., 2025. How do flood risk-socioeconomic interactions influence household income dynamics in shrinking cities of the rust belt? https://doi.org/1 0.2139/ssrn.5205782.
- Knighton, J., Hondula, K., Sharkus, C., Guzman, C., Elliott, R., 2021. Flood risk behaviors of United States riverine metropolitan areas are driven by local hydrology and shaped by race. Proc. Natl. Acad. Sci. 118 (13), e2016839118. https://doi.org/ 10.1073/pnas.2016839118.
- Kousky, C., 2014. Informing climate adaptation: a review of the economic costs of natural disasters. Energy Econ. 46, 576–592. https://doi.org/10.1016/j. energ. 2013.09.029
- Kron, W., 2005. Flood risk = hazard values vulnerability. Water Int. 30 (1), 58–68. https://doi.org/10.1080/02508060508691837.
- Kumar, R., Acharya, P., 2016. Flood hazard and risk assessment of 2014 floods in kashmir valley: a space-based multisensor approach. Nat. Hazards 84 (1), 437–464. https://doi.org/10.1007/s11069-016-2428-4.
- Laidlaw, S., Percival, S., 2024. Flood resilience: a review of evolving definitions. Nat. Hazards 120 (12), 10773–10784. https://doi.org/10.1007/s11069-024-06627-9.
- Li, M., Verburg, P.H., Van Vliet, J., 2022. Global trends and local variations in land take per person. Landsc. Urban Plann. 218, 104308. https://doi.org/10.1016/j. landurbplan.2021.104308.
- Liang, X., Lettenmaier, D.P., Wood, E.F., Burges, S.J., 1994. A simple hydrologically based model of land surface water and energy fluxes for general circulation models. J. Geophys. Res. Atmos. 99 (D7), 14415–14428. https://doi.org/10.1029/94JD00483.
- Ma, S., Wang, L.J., Jiang, J., Zhao, Y.G., 2024. Land use/land cover change and soil property variation increased flood risk in the Black soil region, China, in the last 40 years. Environ. Impact Assess. Rev. 104, 107314. https://doi.org/10.1016/j. eiar.2023.107314.
- Merz, B., Blöschl, G., Vorogushyn, S., Dottori, F., Aerts, J.C.J.H., Bates, P., Bertola, M., Kemter, M., Kreibich, H., Lall, U., Macdonald, E., 2021. Causes, impacts and patterns of disastrous river floods. Nat. Rev. Earth Environ. 2 (9), 592–609. https://doi.org/10.1038/s43017-021-00195-3.
- Njoku, C.G., Efiong, J., Ayara, N.A.N., 2020. A geospatial expose of flood-risk and vulnerable areas in Nigeria. Int. J. Appl. Geospatial Res. (IJAGR) 11 (3), 87–110. https://doi.org/10.4018/IJAGR.20200701.oa1.
- Opperman, J.J., Galloway, G.E., 2022. Nature-based solutions for managing rising flood risk and delivering multiple benefits. One Earth 5 (5), 461–465. https://doi.org/10.1016/j.oneear.2022.04.012.
- Oswalt, P., Rieniets, T., Schirmel, H., 2006, Atlas of Shrinking Cities.
- Pearl River Water Resources Commission of the Ministry of Water Resources, 2015. Comprehensive planning of the pearl river basin, 2012-2030. https://www.pearlwater.gov.cn/zwgkcs/slghn/201903/t20190305_91390.html.
- Qin, X., Qin, X., 2025. Research on the level of high-quality urban development based on big data evaluation system: a study of 151 prefecture-level cities in China. Sustainability 17 (3), 836. https://doi.org/10.3390/su17030836.
- Ramesh, V., Iqbal, S.S., 2022. Urban flood susceptibility zonation mapping using evidential belief function, frequency ratio and fuzzy gamma operator models in GIS: a case study of greater mumbai, Maharashtra, India. Geocarto Int. 37 (2), 581–606. https://doi.org/10.1080/10106049.2020.1730448.
- Rentschler, J., Avner, P., Marconcini, M., Su, R., Strano, E., Vousdoukas, M., Hallegatte, S., 2023. Global evidence of rapid urban growth in flood zones since 1985. Nature 622 (7981), 87–92. https://doi.org/10.1038/s41586-023-06468-9.
- Ronco, M., Tárraga, J.M., Muñoz, J., Piles, M., Marco, E.S., Wang, Q., Espinosa, M.T.M., Ponserre, S., Camps-Valls, G., 2023. Exploring interactions between socioeconomic context and natural hazards on human population displacement. Nat. Commun. 14 (1), 8004. https://doi.org/10.1038/s41467-023-43809-8.
- Shahfahad, Mourya M., Kumari, B., Tayyab, M., Paarcha, A., Asif, Rahman A., 2021. Indices based assessment of built-up density and urban expansion of fast growing surat city using multi-temporal landsat data sets. Geojournal 86 (4), 1607–1623. https://doi.org/10.1007/s10708-020-10148-w.
- Shahtahmassebi, A.R., Song, J., Zheng, Q., Blackburn, G.A., Wang, K., Huang, L.Y., Pan, Y., Moore, N., Shahtahmassebi, G., Sadrabadi Haghighi, R., Deng, J.S., 2016. Remote sensing of impervious surface growth: a framework for quantifying urban expansion and re-densification mechanisms. Int. J. Appl. Earth Obs. Geoinf. 46, 94–112. https://doi.org/10.1016/j.jag.2015.11.007.
- Sohn, W., Kim, J.H., Li, M.H., Brown, R.D., Jaber, F.H., 2020. How does increasing impervious surfaces affect urban flooding in response to climate variability? Ecol. Indic. 118, 106774. https://doi.org/10.1016/j.ecolind.2020.106774.
- Song, X., Feng, Q., Xia, F., Li, X., Scheffran, J., 2021. Impacts of changing urban land-use structure on sustainable city growth in China: a population-density dynamics perspective. Habitat Int. 107, 102296. https://doi.org/10.1016/j. habitatts 2020.102306.
- Sun, Y., Jiao, L., Guo, Y., Xu, Z., 2024. Recognizing urban shrinkage and growth patterns from a global perspective. Appl. Geogr. 166, 103247. https://doi.org/10.1016/j. approgr. 2024.103247.
- Tellman, B., Sullivan, J.A., Kuhn, C., Kettner, A.J., Doyle, C.S., Brakenridge, G.R., Erickson, T.A., Slayback, D.A., 2021. Satellite imaging reveals increased proportion of population exposed to floods. Nature 596 (7870), 80–86. https://doi.org/ 10.1038/s41586-021-03695-w.

- Wang, W., Jiao, L., Zhang, W., Jia, Q., Su, F., Xu, G., Ma, S., 2020. Delineating urban growth boundaries under multi-objective and constraints. Sustain. Cities Soc. 61, 102279. https://doi.org/10.1016/j.scs.2020.102279.
- Ward, P.J., Jongman, B., Aerts, J.C.J.H., Bates, P.D., Botzen, W.J.W., Diaz Loaiza, A., Hallegatte, S., Kind, J.M., Kwadijk, J., Scussolini, P., Winsemius, H.C., 2017. A global framework for future costs and benefits of river-flood protection in urban areas. Nat. Clim. Change 7 (9), 642–646. https://doi.org/10.1038/nclimate3350.
- Wu, J., Gao, X., 2013. A gridded daily observation dataset over China region and comparison with the other datasets. Chin. J. Geophys. 56 (4), 1102–1111. https:// doi.org/10.6038/cjg20130406 (in Chinese).
- Wu, J., Gao, X., Giorgi, F., Chen, D., 2017. Changes of effective temperature and cold/hot days in late decades over China based on a high resolution gridded observation dataset. Int. J. Climatol. 37 (S1), 788–800. https://doi.org/10.1002/joc.5038.
- Xu, Q., Dong, Y., Yang, R., 2018. Urbanization impact on carbon emissions in the pearl river Delta region: kuznets curve relationships. J. Clean. Prod. 180, 514–523. https://doi.org/10.1016/j.jclepro.2018.01.194.
- Yamazaki, D., Kanae, S., Kim, H., Oki, T., 2011. A physically based description of floodplain inundation dynamics in a global river routing model. Water Resour. Res. 47, W04501. https://doi.org/10.1029/2010WR009726.
- Yu, H., Zhao, Y., Fu, Y., 2019. Optimization of impervious surface space layout for prevention of urban rainstorm waterlogging: a case study of guangzhou, China. Int.

- J. Environ. Res. Publ. Health 16 (19), 3613. https://doi.org/10.3390/jierph16193613.
- Zhang, Q., Singh, V.P., Peng, J., Chen, Y.D., Li, J., 2012. Spatial–temporal changes of precipitation structure across the pearl river basin, China. J. Hydrol. 440–441, 113–122. https://doi.org/10.1016/j.jhydrol.2012.03.037.
- Zhang, S., Yi, J., Li, Z., Yang, M., 2022a. Frontiers and trends of blended learning research in China based on visualization analysis of CNKI database. Int. J. Inf. Commun. Technol. Educ. 18 (2), 1–13. https://doi.org/10.4018/ijicte.314566.
- Zhang, S., Zhang, Y., Yu, J., Fan, Q., Si, J., Zhu, W., Song, M., 2022b. Interpretation of the spatiotemporal evolution characteristics of land deformation in beijing during 2003–2020 using sentinel, ENVISAT, and landsat data. Remote Sens. 14 (9), 2242. https://doi.org/10.3390/rs14092242.
- Zhong, M., Zhang, H., Jiang, T., Guo, J., Zhu, J., Wang, D., Chen, X., 2023. A hybrid model combining the cama-flood model and deep learning methods for streamflow prediction. Water Resour. Manag. 37 (12), 4841–4859. https://doi.org/10.1007/s11269.023-03583-0
- Zou, Y., Chen, W., Li, S., Wang, T., Yu, L., Xu, M., Singh, R.P., Liu, C.Q., 2022. Spatio-temporal changes in vegetation in the last two decades (2001–2020) in the beijing-tianjin-hebei region. Remote Sens. 14 (16), 3958. https://doi.org/10.3390/rs14163958